

Article

Characteristics of Coastal Low-Level Jets in the Boundary Layer of the Pearl River Estuary

Zongxu Qiu ¹, Jinhong Xian ^{1,2} , Yuexin Yang ¹, Chao Lu ¹, Honglong Yang ^{1,*}, Yuanyuan Hu ¹ , Jiaqi Sun ¹ and Chunsheng Zhang ¹

¹ Shenzhen National Climate Observatory, Meteorological Bureau of Shenzhen Municipality, Shenzhen 518040, China; qq_qzx@126.com (Z.Q.); jhxian@mail.ustc.edu.cn (J.X.); yyx_lightning@163.com (Y.Y.); luchao@weather.sz.gov.cn (C.L.); huyuanyuan@weather.sz.gov.cn (Y.H.); wyojsun@163.com (J.S.); zhangchunsheng@weather.sz.gov.cn (C.Z.)

² School of Atmospheric Sciences, Nanjing University, Nanjing 210023, China

* Correspondence: yanghl01@163.com

Abstract: It is well-known that coastal low-level jets (CLLJs) play an essential role in transporting heat, water vapor and pollutants. However, the CLLJ characteristics in the Pearl River Estuary have not been deeply revealed due to the lack of long-term observations. Based on the long-term observations from a wind lidar, we analyze the primary climatic characteristics of the CLLJs in the Pearl River Estuary and investigate their relationships with large-scale and local-scale synoptic systems. The results show that the CLLJs mainly appear during the flood season, with the most occurrence in May. The CLLJ occurrence during the flood season is mainly influenced by the large-scale north–south pressure gradient driven by the western Pacific subtropical high and terrestrial low-pressure systems. The occurrence of the CLLJs exhibits a distinct diurnal cycle with two different peaks in different seasons. One peak appears at nighttime, mainly during non-flood seasons. The other appears in the afternoon, mainly during the flood season. In the non-flood seasons, under the influence of cold air, the inertial oscillations triggered by the land–sea thermal contrast lead to CLLJ onset at nighttime in the Pearl River Estuary. During the flood season, the strong near-surface pressure gradient contributes to CLLJ onset in the afternoon, while the topography (blocking and passing) is more conducive to the occurrence of the CLLJs in the Pearl River Estuary. These findings reveal the formation mechanisms of the CLLJs over the Pearl River Estuary, thus providing a basis for further understanding the precipitation in the Pearl River Estuary and the occurrence of the CLLJs in other coastal areas with complex mountain ranges.

Keywords: coastal low-level jet; wind lidar; synoptic condition; Pearl River Estuary



Citation: Qiu, Z.; Xian, J.; Yang, Y.; Lu, C.; Yang, H.; Hu, Y.; Sun, J.; Zhang, C. Characteristics of Coastal Low-Level Jets in the Boundary Layer of the Pearl River Estuary. *J. Mar. Sci. Eng.* **2023**, *11*, 1128. <https://doi.org/10.3390/jmse11061128>

Academic Editor: Alfredo L. Aretxabaleta

Received: 22 April 2023

Revised: 22 May 2023

Accepted: 25 May 2023

Published: 26 May 2023



Copyright: © 2023 by the authors. Licensee MDPI, Basel, Switzerland. This article is an open access article distributed under the terms and conditions of the Creative Commons Attribution (CC BY) license (<https://creativecommons.org/licenses/by/4.0/>).

1. Introduction

In China, carbon neutrality has become a national strategy. In this context, the development of wind energy resources in coastal areas has become more and more common, especially for wind power generation, which is the main way of new energy utilization in coastal areas [1,2]. Understanding the characteristics of wind is an important prerequisite for wind power generation. Wind speeds in the optimum range can carry energy to drive wind turbines, while excessively intense wind speed can easily damage wind turbines. In coastal areas, typhoons and severe convective weather are the main sources of destructive gales. Compared with systemic disaster weather such as typhoons and severe convection, coastal low-level jets (CLLJs) occur more frequently. A thorough understanding of CLLJ characteristics is conducive to analyzing and judging several important engineering issues for wind power generation in coastal areas.

CLLJs are a type of low-level jet (LLJ) that generally occur in the offshore areas of coastal regions [3]. The CLLJs can provide abundant water vapor conditions and unstable energy for precipitation processes to promote heavy rainfall events, thereby affecting the

regional water cycle [4,5]. In addition, they may influence regional pollution events [6]. The CLLJs have been widely studied worldwide due to their important role in regional coastal meteorology.

At present, due to the lack of long-term observations on seas, most studies focused on the spatio-temporal distributions of the CLLJs were based on reanalysis data and numerical simulations [7–9]. Winant et al. showed that the CLLJs are more prone to occur in mid-latitude eastern Chinese seas due to strong cold ocean currents [10]. Ranjha et al. analyzed the global distribution of the CLLJs based on the European Center for Medium-Range Weather Forecasts (ERA-Interim) reanalysis data, and they found a large number of regions with a high frequency of the CLLJs [3]. Probably due to the strict identification criteria of the CLLJs and low spatio-temporal resolutions of reanalysis data, the CLLJs have not been found in China. Recently, some researchers conducted detailed investigations on the CLLJs in the southeast coast of China, the Bohai Sea, the Yellow Sea and the Beibu Gulf of the South China Sea using numerical models [7,9,11,12]. For example, based on a climate model, Li et al. depicted that the CLLJs in the Bohai Sea and the Yellow Sea have strong interannual, annual and diurnal variabilities [12]. Wei et al. analyzed the variation characteristics of the CLLJs in coastal cities, i.e., Tianjin and Shanghai, based on observation data [13].

The formation mechanisms of the LLJs have been discussed in many previous studies, and two main theories have been summarized. One is the inertial oscillation theory, i.e., the weakening of the turbulence mixing effect at night leads to an imbalance between the Coriolis force and the pressure-gradient force, thereby resulting in the inertial oscillation of low-level wind and, thus, the LLJs [14]. The other is the baroclinic theory of sloping terrain, which emphasizes the effect of heating and cooling of sloping terrain on the diurnal variation in boundary-layer wind field [15]. Actually, most recent studies have pointed out that the formation and development of the LLJs are influenced by multiple mechanisms [7,16]. Compared with the LLJs at night, the CLLJs differ in their formation and development mechanisms, which are influenced by more factors. The inertial oscillation caused by the land-sea thermal difference is an important factor affecting the CLLJs [3,17,18]. In addition to inertial oscillations triggered by land-sea thermal differences, coastal terrain is also an essential factor influencing the CLLJs [19,20], as coastal terrain may alter the direction of airflows or accelerate airflows [21,22]. For example, Du et al. analyzed the characteristics of the CLLJs in the Taiwan Strait using high-resolution model data, and they found that the main factor affecting the CLLJs is the land-sea thermal difference, while terrain effects also play a secondary role in CLLJ development [7]. Zhang et al. used high-resolution model data to study a CLLJ along the Bohai Sea coast, and the results indicated that the inertial oscillation caused by the land-sea thermal difference led to the formation of a nocturnal CLLJ in the Bohai Sea [9].

Although significant progress has been made in the field of the CLLJs, there is still a lack of research based on long-term observations, which is undoubtedly detrimental to a more comprehensive understanding of CLLJ issues. Since the LLJs frequently occur in coastal areas and are critical to both wind energy exploitation and disaster prevention, it is necessary to conduct systematic research on the CLLJs based on long-term observation data. Fortunately, the abundant resources of meteorological observation equipment in the Pearl River Estuary area make it possible to achieve this goal [23].

The Pearl River Delta is located in the low latitudes in the south of China's mainland, whose southeast is adjacent to the ocean. The topography of the Pearl River Delta is high in the north and low in the south, with various mountains, hills and a winding coastline. Furthermore, the Pearl River Delta has been one of the most active areas of economic development and industrial production in China's mainland since the reform and opening up, and it can be considered one of the fastest-growing regions in the process of global urbanization in the past 40 years [24]. Currently, it has formed a huge urban agglomeration with a total population of over 70 million. Due to the complex topography, sea-land differences and monsoons, the Pearl River Delta is highly susceptible to gales and

regional pollution, which can cause major losses to economic construction and people's lives and properties. Limited studies have shown that the LLJs occasionally occur in the Pearl River Delta [25,26], affecting not only regional precipitation [27,28], but also regional pollution [6]. There are relatively few systematic observational studies on the CLLJs due to the limitation of observation data on ocean surfaces. Therefore, based on the data from the wind lidar located on the coastal Xiya Island, we investigate the climatic characteristics and the formation and development mechanisms of the CLLJs in the Pearl River Delta in this study, which is of great significance to the local navigation and port services, aviation safety and urban disaster prevention.

The remainder of this paper is organized as follows. The data and methods are provided in Section 2. Section 3 describes the general characteristics and formation mechanisms of the CLLJs. Finally, the conclusions are presented in Section 4.

2. Data and Methods

In this study, the wind lidar (113.81° E, 22.55° N) on Xiya Island (2 km from the shore) along the coast of Shenzhen was used to analyze the CLLJ characteristics, as shown in Figure 1. The wind lidar is produced by Shenzhen Darsunlaser Tech Co., Ltd. (Shenzhen, China) (Table 1). For wind speed and direction, the instrument has a detection height range of 30–1200 m and a vertical resolution of 15 m. The data used in the study cover the period from 1 January to 31 December 2021, with a temporal resolution of 60 s.

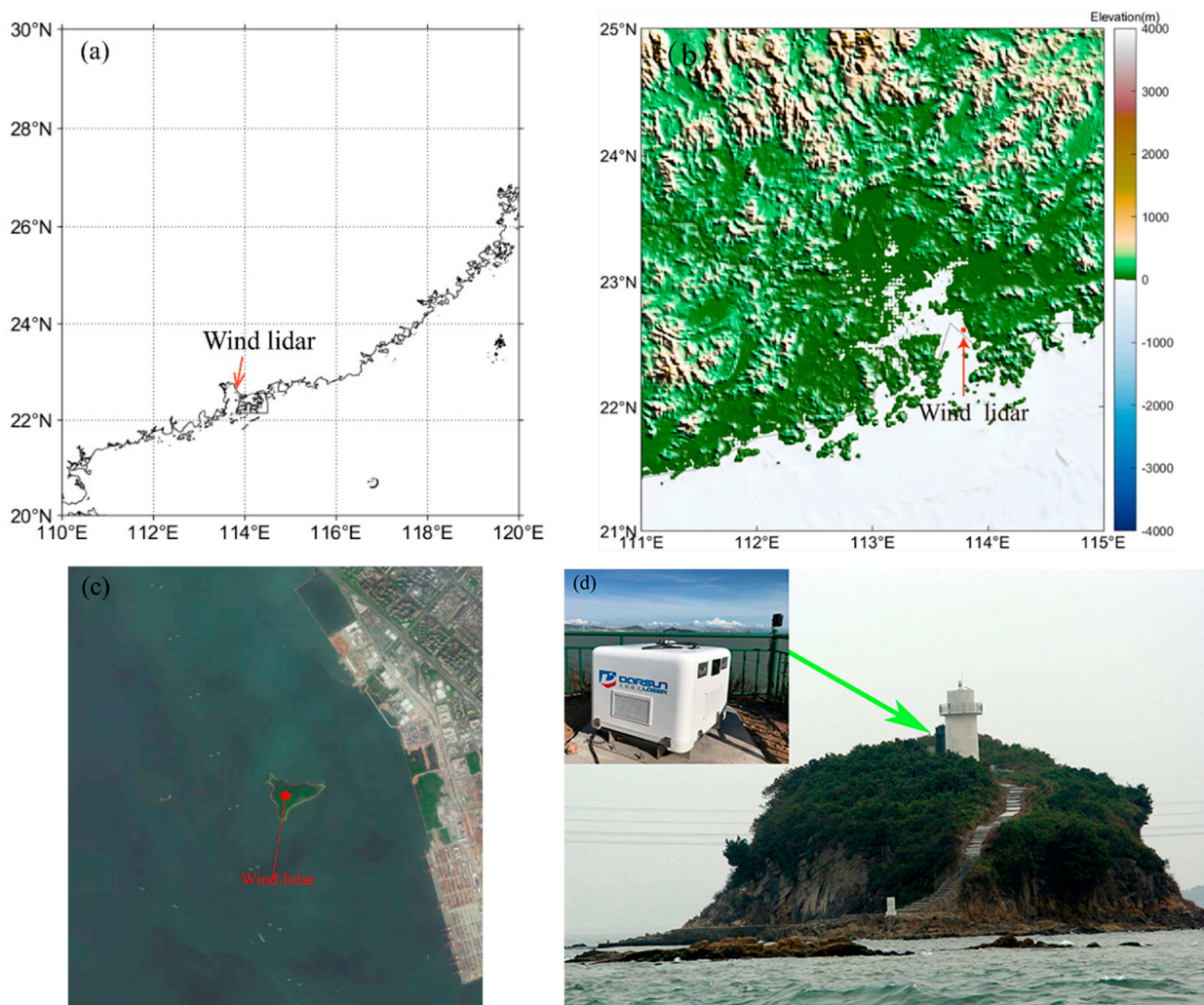


Figure 1. (a–c) Locations and (d) real pictures of the wind lidar.

Table 1. Performance parameters of the wind lidar.

Metrics	Technical Performance Requirements
Blind zone	$\leq 30\text{ m}$
Distance resolution	15 m
Temporal resolution of wind profile	1 min
Errors of wind speed measurement (standard deviation)	$\leq 0.3\text{ m s}^{-1}$
Errors of wind direction measurement (root mean squared error)	$\leq 3^\circ$
Range of radial wind speed measurement	$\pm 37.5\text{ m s}^{-1}$
Range of vertical wind speed measurement	$0\text{--}60\text{ m s}^{-1}$
Range of wind direction measurement	$0^\circ\text{--}360^\circ$
Resolution of radial wind speed	$\leq 0.1\text{ m s}^{-1}$
Wind speed resolution	$\leq 0.1\text{ m s}^{-1}$
Wind direction resolution	$\leq 0.1^\circ$

In order to ensure the reliability of observations, the wind speed measurements were examined overall for every two consecutive levels per day, and the wind speed measurements that deviate by more than two standard deviations from the mean were rejected. For wind profiles, if the missing data exceeded 20% below 500 m, the entire profile was excluded. Then, a linear interpolation method was used to estimate discontinuous or missing values.

Because of the differences in height, range, wind intensity and horizontal and vertical shear of the LLJs, there is no uniform standard for defining the LLJs as yet. The criterion used by Blackadar is $\Delta V = V_{\max} - V_{\min} \geq 2.6\text{ m s}^{-1}$, where V_{\max} indicates the maximum wind speed appearing on the profile, and V_{\min} denotes the minimum wind speed immediately above V_{\max} [14]. Bonner defined the LLJs according to the following four criteria [29]: (1) $V_{\max} \geq 10\text{ m s}^{-1}$ and $\Delta V \geq 2.6\text{ m s}^{-1}$, (2) $V_{\max} \geq 12\text{ m s}^{-1}$ and $\Delta V \geq 6\text{ m s}^{-1}$, (3) $V_{\max} \geq 16\text{ m s}^{-1}$ and $\Delta V \geq 8\text{ m s}^{-1}$ and (4) $V_{\max} \geq 20\text{ m s}^{-1}$ and $\Delta V \geq 10\text{ m s}^{-1}$. Referring to the above criteria, we define the CLLJs in this study according to the criteria, i.e., the maximum of wind speed occurs below 500 m, $V_{\max} \geq 8\text{ m s}^{-1}$ and $\Delta V = V_{\max} - V_{\min} \geq 2.6\text{ m s}^{-1}$, where V_{\min} denotes the minimum wind speed in the vertical profile above the height of V_{\max} . Based on the above criteria, we selected the CLLJs from observations in a year and then performed a statistical analysis. Specifically, we calculated the vertical profile for each minute, and if the above conditions were satisfied for more than 10 min, it was counted as one CLLJ event. If the time interval between two CLLJs was within 30 min, they were counted as the same CLLJ.

3. Results and Discussion

3.1. General Characteristics

3.1.1. Occurrence Frequency and Vertical Structure

The data for the whole year of 2021 were processed according to the method mentioned in Section 2. There were a total of 47,304 samples, and each sample lasted 10 min. A total of 806 CLLJ events were identified during the year. The statistical characteristics of the CLLJs are presented in Figure 2a.

As shown in Figure 2a, the CLLJs in Shenzhen exhibit obvious seasonal variations and can occur in any month of the year. The occurrence frequency is the highest in May, with 27 days and a total of 26.5 h, followed by June. The lowest frequency is in November, with 10 days and a total of 3.2 h, that is, the average duration of each CLLJ is 0.3 h. The wind speed at the centers of the CLLJs varies between 8 m s^{-1} and 25 m s^{-1} , with an average of 16.4 m s^{-1} . The wind speed at the centers of most of the CLLJs is below 14 m s^{-1} (accounting for 95%). The wind direction at the centers of the CLLJs shows a double-peak distribution, with the first peak mainly from the southerly direction (accounting for 45%) and the second peak from the easterly–southeasterly direction (accounting for 29%). The CLLJs also occur in other wind directions, but the frequency is low. Regarding the duration of the CLLJs, more than half of all 806 CLLJ events during the year lasted less than one

hour. Overall, the proportion of the CLLJs with a longer duration is smaller, and this trend is consistent in all months and all seasons.

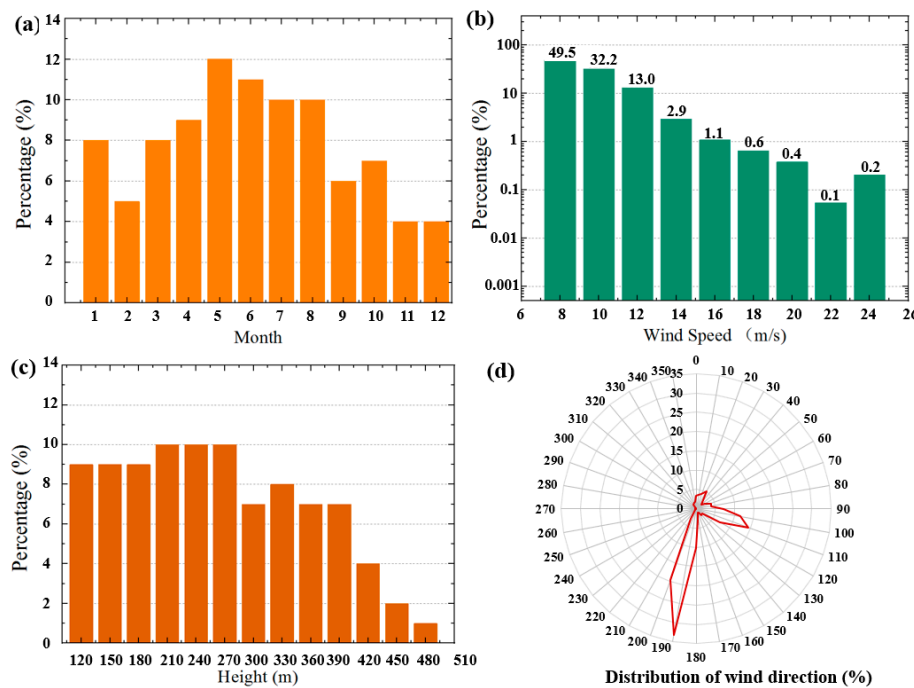


Figure 2. Statistics of the (a) occurrence frequency, (b) wind speed, (c) height and (d) wind direction of the ultra-low-level jets (CLLJs).

Although the maximum wind speed at the CLLJ centers may appear at any height, it is prone to appear at a specific height range (Figure 2c). In this study, the peak of the maximum wind speed shows a double-peak distribution, and the two peaks are mainly in 150–250 m and 300–400 m, accounting for 41% and 31%. Further analysis of the wind speed and height of CLLJ centers revealed that large-value regions of the wind speed at jet centers tend to occur between 250 m and 400 m. According to local news reports, there are 158 skyscrapers with a height of more than 200 m in Shenzhen as of October 2021, ranking the first worldwide in terms of the number. Therefore, the CLLJs not only pose a threat to wind power generation in coastal areas, but are also critical to the safety of the wind environment associated with urban buildings.

3.1.2. Seasonal and Diurnal Variations

Shenzhen is located in the subtropical monsoon climate zone of South China, and the climatic characteristics of the four seasons are not obvious. According to the standards of the local meteorological departments, the year is generally divided into dry (non-flood) and wet (flood) seasons, i.e., April–September is classified as the wet season, and January–March and October–December are regarded as the dry seasons. During the wet season, the CLLJs occur almost every 1.3 days on average, with 141 days (99 h) in total. During the dry seasons, the CLLJs have a relatively low frequency, totaling 80 days.

The diurnal variation in the occurrence frequency of the CLLJs is further investigated. As shown in Figure 3, the diurnal variations in the CLLJ occurrence frequency in the wet and dry seasons are clearly different. Specifically, the CLLJ frequency in the wet season is the highest during 12:00–22:00 LST, while the diurnal variation in the CLLJs during the dry seasons shows a “U”-shaped distribution, with the highest frequency in the early morning and at midnight. Moreover, the wind direction at the CLLJ centers is dominated by a southerly wind during the wet season, while this is an easterly wind during the dry seasons. The different diurnal variation characteristics of the CLLJs in different seasons indicate that the CLLJs in Shenzhen are not only related to the diurnal variation in the

boundary layer, but also linked to specific weather systems in different seasons, such as cold air and western Pacific subtropical high (WPSH).

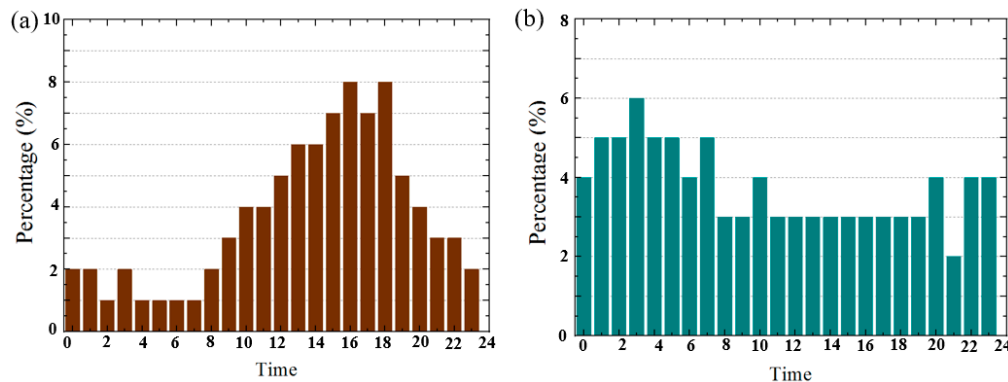


Figure 3. Diurnal variations in the CLLJs in the (a) wet season and (b) dry season.

3.2. Formation Mechanisms

In order to further explore the relationship between CLLJ formation and synoptic systems in Shenzhen, a statistical analysis of the synoptic systems on days with CLLJs was performed. The results show that there were 221 days with the CLLJs in Shenzhen during 2020, of which there were 152 days with the CLLJs related to the WPSH and 69 days with the CLLJs associated with cold air. The CLLJs influenced by cold air occur mainly during October–December and January–March, while the CLLJs associated with the WPSH appear mainly during April–September.

3.2.1. Cold Air

The height-time cross-sections of the wind velocity (Figure 4) indicate that the CLLJs last from midnight to early morning at the height of 400 m AGL. During the daytime, the CLLJs disappear as the planetary boundary layer (PBL) rises. By late afternoon, the CLLJs redevelop as the PBL height decreases. These diurnal variations in the CLLJs and PBL are consistent with the theory proposed by Blackadar, i.e., the formation and dissipation of the CLLJs are regulated by the diurnal variation in the PBL [14]. The East Asian major trough deepens noticeably and becomes stable, accompanied by a remarkable weakening of the WPSH and an intense cold-air outbreak on the ground. At this time, Shenzhen is under the control of a strong cold high-pressure ridge. In this context, there is a strong pressure gradient from the northeast to the southwest of the Pearl River Delta, resulting in large-scale northerly wind reaching Shenzhen (Figure 5). Previous studies have shown that the land–sea thermal contrast can lead to thermodynamic circulations along the coast [11,30]. As presented in Figure 6, due to the heating of the land in Shenzhen by solar radiation, the temperature difference between the land and the ocean increases in the afternoon. A thermodynamic circulation (there are downdrafts over the land with a low-level horizontal wind blowing toward the land) is triggered around noon and then intensified due to the continuous heating by solar radiation over land until sunset. Due to inertial oscillations, the ageostrophic wind rotates clockwise. At midnight, the southerly wind enhances the background wind in Shenzhen (Figure 4). Hence, this inertial oscillation mechanism explains the occurrence of the CLLJs at night during the non-flood seasons [14], similar to the diurnal variations in the CLLJs in the Taiwan Strait and the Bohai Sea [7,9].

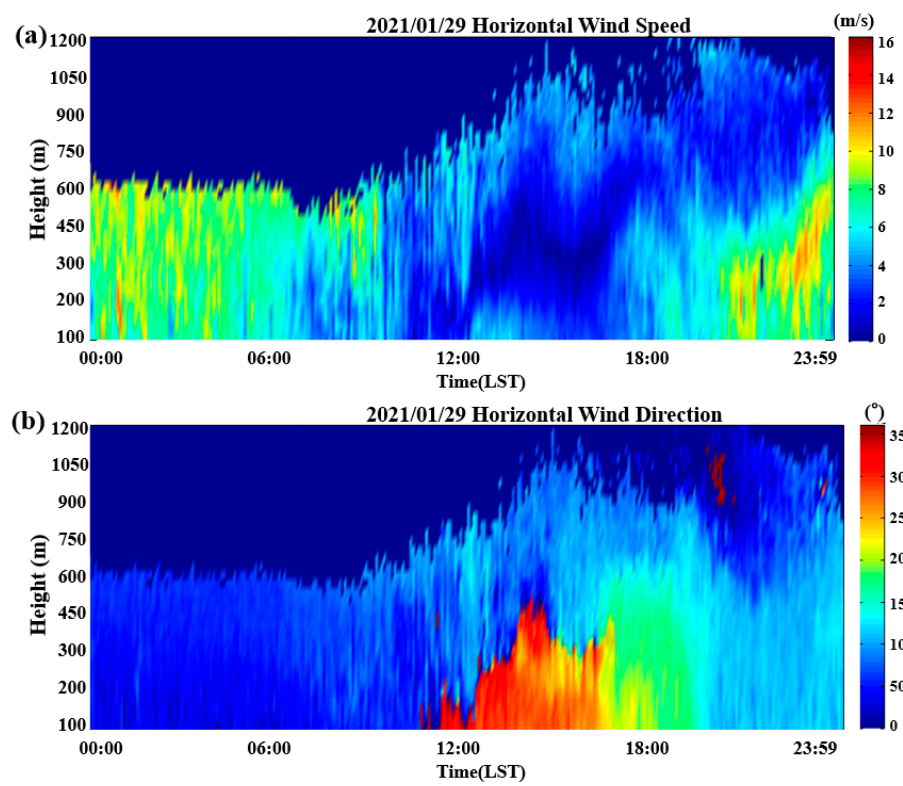


Figure 4. Diurnal variations in (a) wind speed and (b) direction observed on Xiya Island on 29 January 2021.

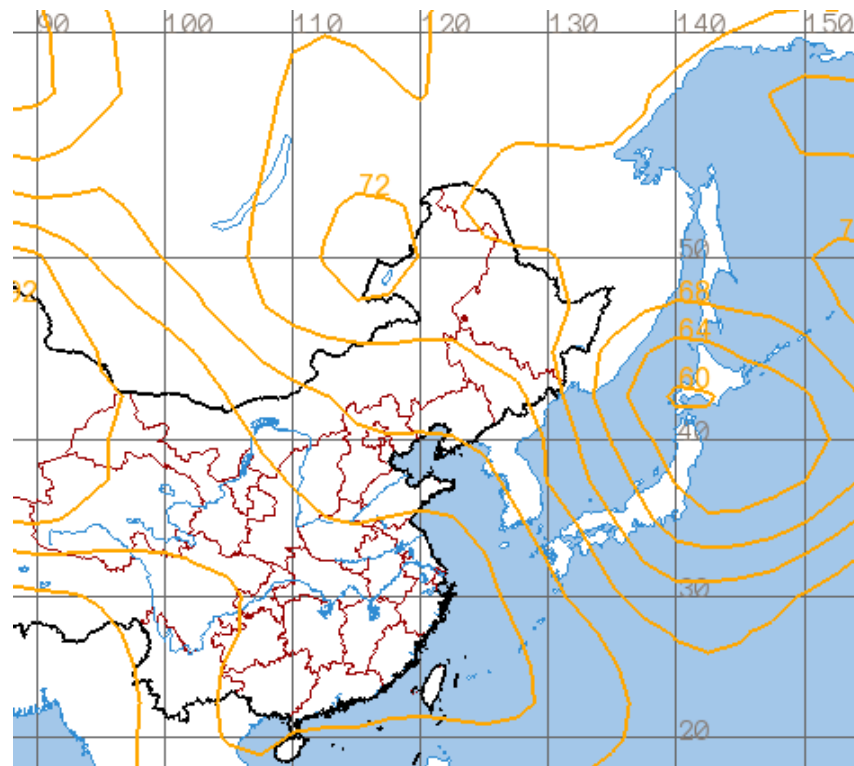


Figure 5. Distribution of the 925 hPa geopotential height on 29 January 2021.

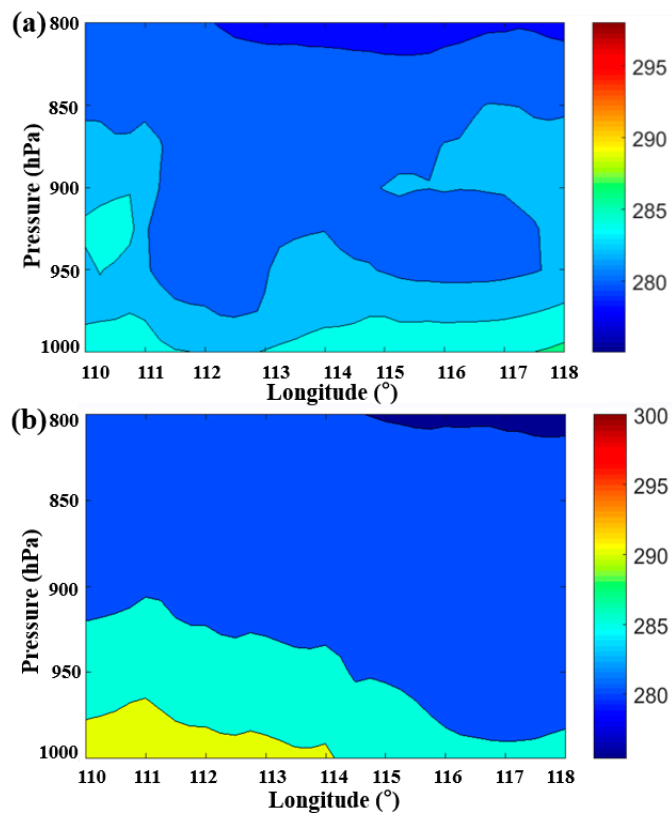


Figure 6. Vertical temperature cross-sections (a) at 09:00 LST and (b) at 16:00 LST on 29 January 2021 (the data from the ECMWF).

3.2.2. Western Pacific Subtropical High

The diurnal variation in the CLLJs during the flood season differs considerably from that during the non-flood seasons. Therefore, the CLLJs during the flood season cannot be briefly explained by the land-sea thermal contrast and inertial oscillations. Zhang et al. investigated the formation mechanisms of the afternoon CLLJs in the Liaodong Bay of the Bohai Sea, and they found that the influence of topography makes an important contribution to the formation of the CLLJs [9]. This research provides a meaningful reference for the cases in this study. Figure 7 presents a typical case associated with the WPSH. Obviously, the CLLJ case shows an obvious diurnal variation on May 20, mainly occurring during 12:00–18:00 LST. On that day, the WPSH was located in the northern South China Sea, and a low-pressure system exists in the north of Shenzhen, resulting in the Pearl River Estuary being located at the northern edge of the WPSH and an obvious north-south pressure gradient over it (Figure 8). As shown in Figure 1, a large number of hilly mountains exist on the periphery of the Pearl River Estuary, and the mountains are mostly below 500 m. In terms of solar radiation, sloping topography can change the horizontal distribution of radiation heating rates on the surface [31]. The sloping mountain surface can receive more solar radiation in the afternoon and, thus, the atmospheric baroclinity below the mountain height is further enhanced by the heating effect. Corresponding to the thermal wind mechanism, the geostrophic wind in the afternoon decreases from the surface to the upper levels. Since vertical wind shear is one of the important criteria for judging the CLLJs, this vertical distribution of the geostrophic wind favors the occurrence of CLLJ events. In the perspective of hydromechanics, the windward terrain can act as a barrier, and it is difficult for airflow below a certain height to cross the mountain tops. Thus, the airflows blowing landward from the southwestern sea surface below a certain height are primarily blocked by the mountains on the eastern coast of the Pearl River Estuary, which favors the formation of a shallow high-pressure region near the lower layers of the

mountains, resulting in an imbalance of the horizontal pressure gradient force with the Coriolis force and frictional force in lower levels [32]. In this case, the geostrophic wind starts to accelerate under the effect of the geostrophic adjustment. Through this process, the wind within the Pearl River Estuary is deflected and eventually aligned with the mountains. The near-surface coastal wind parallel to the coast favors the development of the CLLJs [3]. Consequently, a “blocking jet” is generated in the lower levels of the mountains.

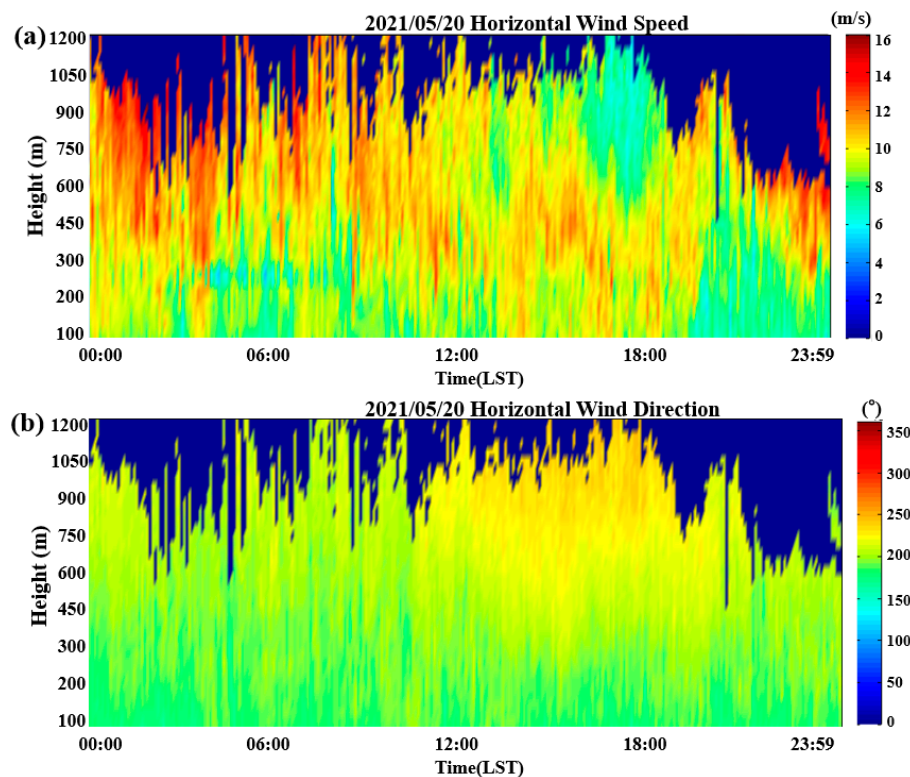


Figure 7. Diurnal variations in the (a) wind speed and (b) direction observed on Xiya Island on 20 May 2021.

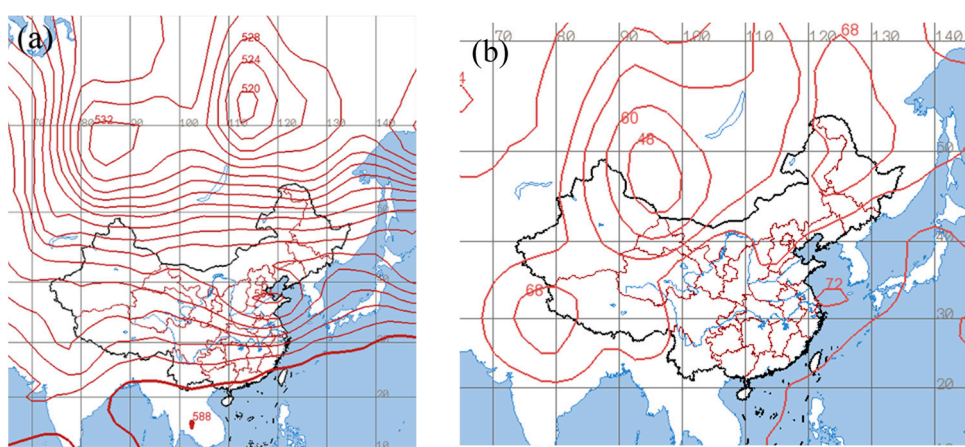


Figure 8. Distributions of the (a) 500 hPa and (b) 925 hPa geopotential height on 20 May 2021.

This formation mechanism of the CLLJs due to the background of the WPSH just explains the relatively high frequency of the CLLJs during the pre-flood period and the relatively low frequency of the CLLJs during the post-flood period. During the pre-flood period (April–June), the low-pressure system in northern Japan moves eastward rapidly, and the East Asian major trough also moves eastward. Additionally, the East Asian

atmospheric circulation becomes relatively flat, the WPSH is located in the northern South China Sea, and a low-pressure system exists in the north. There is a southerly wind on the surface. In this circulation background, the near-surface coastal wind parallel to the coast favors the development of the CLLJs [3]. During the post-flood period (July–September), the WPSH further strengthens and extends westward, and the Pearl River Delta region is controlled by the WPSH ridge. Moreover, the low-level wind rotates counterclockwise and eventually has a strong component that blows toward the coastline. Since the CLLJs tend to appear when the background wind blows along the coastline, the wind direction during the post-flood period may hinder the development of the CLLJs. As a result, the frequency of the CLLJs decreases during the post-flood period.

4. Conclusions

Based on the long-term observations from the wind lidar, the climatic characteristics and formation mechanisms of the CLLJs in the Pearl River Delta are investigated in this study, and the synoptic situation associated with the CLLJ formation is analyzed and determined. Additionally, the main diurnal variation characteristics of the CLLJs in the Pearl River Delta are clarified. The main conclusions are as follows.

Long-term observations (January 2021 to December 2021) in Shenzhen indicate the characteristics of the occurrence frequency, vertical structure and seasonal and diurnal variations in the CLLJs. The CLLJs occur on more than 60% of the days of the year, and their maximum wind speed appears mainly at the height of 150–250 m.

In terms of seasonal variation, the CLLJs occur mainly during the flood season and have a low frequency during the non-flood seasons, with the most occurrence in May. This seasonal variation in the CLLJ frequency may be related to certain synoptic systems that occur frequently during these specific seasons. The occurrence of the CLLJs during the flood season is influenced by the large-scale horizontal pressure gradient driven by the WPSH and terrestrial low-pressure systems. In this context, the CLLJs tend to occur when the background wind is a strong southerly wind. In contrast, the occurrence of CLLJs during the non-flood seasons is mainly influenced by the large-scale pressure gradient generated by the impact of cold air.

There are differences in the diurnal variations and driving mechanisms of the CLLJs between the flood and non-flood seasons. During the non-flood seasons, the CLLJs occur mainly at nighttime and in the early morning, and the inertial oscillation triggered by the land–sea thermal contrast is the main reason for the diurnal variation in CLLJs. During the flood season, the CLLJs are generated at 12:00 LST and disappear at 21:00 LST. The slope of the Pearl River Delta enhances the solar radiation gradient on the surface and, thus, the atmospheric baroclinity is more pronounced. The strong near-surface pressure gradient contributes to the afternoon CLLJs, while the topography (blocking and passing) is more conducive to the occurrence of the CLLJs in the Pearl River Estuary.

Author Contributions: Conceptualization, Z.Q. and H.Y.; methodology, Z.Q.; software, J.X.; validation, J.X., Y.Y. and Z.Q.; formal analysis, Z.Q.; investigation, J.S.; resources, C.L.; data curation, Y.H.; writing—original draft preparation, Z.Q.; writing—review and editing, Z.Q.; visualization, C.Z.; supervision, H.Y.; project administration, H.Y.; funding acquisition, H.Y. All authors have read and agreed to the published version of the manuscript.

Funding: This work was supported by the Special Project for Sustainable Development of Shenzhen (Grant No. KCXFZ20201221173412035), the National Natural Science Foundation of China (Grant No. 42275065), the Guangdong Province Science and Technology Department Project (Grant No. 2021B1212050024), Scientific research projects of Guangdong Provincial Meteorological Bureau (Grant No. GRMC2020M29) and the Science and Technology Innovation Team Plan of Guangdong Meteorological Bureau (Grant No. GRMCTD202003).

Institutional Review Board Statement: Not applicable.

Informed Consent Statement: Not applicable.

Data Availability Statement: Data underlying the results presented in this paper are not publicly available at this time, but may be obtained from the authors upon reasonable request.

Acknowledgments: The authors are thankful for the data support from the European Centre for Medium-Range Weather Forecasts (ECMWF).

Conflicts of Interest: The authors declare no conflict of interest.

References

1. Zheng, C.W.; Li, C.Y.; Pan, J.; Liu, M.Y.; Xia, L.L. An overview of global ocean wind energy resource evaluations. *Renew. Sustain. Energy Rev.* **2016**, *53*, 1240–1251. [[CrossRef](#)]
2. Zhou, A.; He, M.; Zhu, R.; Cheng, X. Numerical Simulation of the Development Potential of Wind Energy Resources over China's Offshore Areas. *Resour. Sci.* **2010**, *32*, 1434–1443.
3. Ranjha, R.; Svensson, G.; Tjernström, M.M.; Semedo, A. Global distribution and seasonal variability of coastal low-level jets derived from ERA-Interim reanalysis. *Tellus Ser. A* **2013**, *65*, 20412. [[CrossRef](#)]
4. Liu, H.; He, M.; Wang, B.; Zhang, Q. Advances in Low-Level Jet Research and Future Prospects. *J. Meteorol. Res.* **2014**, *72*, 191–206. [[CrossRef](#)]
5. Du, Y.; Chen, G. Climatology of Low-Level Jets and Their Impact on Rainfall over Southern China during the Early-Summer Rainy Season. *J. Clim.* **2019**, *32*, 8813–8833. [[CrossRef](#)]
6. Yang, H.; Lu, C.; Hu, Y.; Chan, P.; Li, L.; Zhang, L. Effects of Horizontal Transport and Vertical Mixing on Nocturnal Ozone Pollution in the Pearl River Delta. *Atmosphere* **2022**, *13*, 1318. [[CrossRef](#)]
7. Du, Y.; Chen, Y.; Zhang, Q. Numerical Simulations of the Boundary Layer Jet off the Southeastern Coast of China. *Mon. Weather Rev.* **2015**, *143*, 1212–1231. [[CrossRef](#)]
8. Ranjha, R.; Tjernström, M.; Semedo, A.; Svensson, G.; Cardoso, R.M. Structure and variability of the Oman coastal low-level jet. *Tellus A Dyn. Meteorol. Oceanogr.* **2015**, *67*, 25285. [[CrossRef](#)]
9. Zhang, F.; Zhang, Q.; Du, Y.; Kong, H. Characteristics of Coastal Low-Level Jets in the Bohai Sea, China, during the Early Warm Season. *J. Geophys. Res. Atmos.* **2018**, *123*, 13763–13774. [[CrossRef](#)]
10. Winant, C.D.; Dorman, C.E.; Friehe, C.A.; Beardsley, R.C. The Marine Layer off Northern California: An Example of Supercritical Channel Flow. *J. Atmos. Sci.* **1988**, *45*, 3588–3605. [[CrossRef](#)]
11. Kong, H.; Zhang, Q.; Du, Y.; Zhang, F. Characteristics of Coastal Low-Level Jets over Beibu Gulf, China, During the Early Warm Season. *J. Geophys. Res. Atmos.* **2020**, *125*, e2019JD031918. [[CrossRef](#)]
12. Li, D.; von Storch, H.; Yin, B.; Xu, Z.; Qi, J.; Wei, W.; Guo, D. Low-Level Jets Over the Bohai Sea and Yellow Sea: Climatology, Variability, and the Relationship with Regional Atmospheric Circulations. *J. Geophys. Res. Atmos.* **2018**, *123*, 5240–5260. [[CrossRef](#)]
13. Wei, W.; Zhang, H.S.; Ye, X.X. Comparison of low-level jets along the north coast of China in summer. *J. Geophys. Res. Atmos.* **2015**, *119*, 9692–9706. [[CrossRef](#)]
14. Blackadar, A.K. Boundary layer wind maxima and their significance for the growth of nocturnal inversions. *Bull. Amer. Meteor. Soc.* **1957**, *5*, 283–290. [[CrossRef](#)]
15. Holton, J.R. The diurnal boundary layer wind oscillation above sloping terrain. *Tellus* **2010**, *19*, 199–205. [[CrossRef](#)]
16. Jiang, X.; Lau, N.; Held, I.M.; PLoShay, J.J. Mechanisms of the Great Plains Low-Level Jet as Simulated in an AGCM. *J. Atmos. Sci.* **2007**, *64*, 532–547. [[CrossRef](#)]
17. Parish, T.R. Forcing of the Summertime Low-Level Jet along the California Coast. *J. Appl. Meteorol.* **2000**, *39*, 2421–2433. [[CrossRef](#)]
18. Petenko, I.; Casasanta, G.; Bucci, S.; Kallistratova, M.; Argentini, S. Turbulence, Low-Level Jets, and Waves in the Tyrrhenian Coastal Zone as Shown by Sodar. *Atmosphere* **2019**, *11*, 28. [[CrossRef](#)]
19. Yeh, H.C.; Chen, Y.L. Numerical Simulations of the Barrier Jet over Northwestern Taiwan during the Mei-Yu Season. *Mon. Weather Rev.* **2003**, *131*, 1396–1407. [[CrossRef](#)]
20. Chen, Y.; Li, J. Characteristics of Surface Airflow and Pressure Patterns over the Island of Taiwan during TAMEX. *Mon. Weather Rev.* **1995**, *123*, 695–716. [[CrossRef](#)]
21. Ridgway, K.R.; Dunn, J.R. Mesoscale structure of the mean East Australian Current System and its relationship with topography. *Prog. Ocean.* **2003**, *56*, 189–222. [[CrossRef](#)]
22. Lin, P.; Chen, Y.; Chen, C.; Liu, C.; Chen, C. Numerical experiments investigating the orographic effects on a heavy rainfall event over the northwestern coast of Taiwan during TAMEX IOP 13. *Meteorol. Atmos. Phys.* **2011**, *114*, 35. [[CrossRef](#)]
23. Li, L.; Chan, P.W.; Deng, T.; Yang, H.; Luo, H.; Xia, D.; He, Y. Review of advances in urban climate study in the Guangdong-Hong Kong-Macau Greater Bay Area, China. *Atmos. Res.* **2021**, *261*, 105759. [[CrossRef](#)]
24. Hui, E.C.M.; Li, X.; Chen, T.; Lang, W. Deciphering the spatial structure of China's megacity region: A new bay area—The Guangdong-Hong Kong-Macao Greater Bay Area in the making. *Cities* **2020**, *105*, 102168. [[CrossRef](#)]
25. Miao, Y.; Guo, J.; Liu, S.; Wei, W.; Zhang, G.; Lin, Y.; Zhai, P. The Climatology of Low-Level Jet in Beijing and Guangzhou, China. *J. Geophys. Res. Atmos.* **2018**, *123*, 2816–2830. [[CrossRef](#)]
26. Shu, Z.R.; Li, Q.S.; He, Y.C.; Chan, P.W. Investigation of low-level jet characteristics based on wind profiler observations. *J. Wind Eng. Ind. Aerod.* **2018**, *174*, 369–381. [[CrossRef](#)]

27. Du, Y.; Chen, G. Heavy Rainfall Associated with Double Low-Level Jets over Southern China. Part I: Ensemble-Based Analysis. *Mon. Weather Rev.* **2018**, *146*, 3827–3844. [[CrossRef](#)]
28. Zhang, M.; Meng, Z. Warm-Sector Heavy Rainfall in Southern China and Its WRF Simulation Evaluation: A Low-Level-Jet Perspective. *Mon. Weather Rev.* **2019**, *147*, 4461–4480. [[CrossRef](#)]
29. Bonner, W.D. Climatology of the low level jet. *Mon. Weather Rev.* **1968**, *96*, 833–850. [[CrossRef](#)]
30. Atkins, N.T.; Wakimoto, R.M.; Weckwerth, T.M. Observations of the Sea-Breeze Front during CaPE. Part II: Dual-Doppler and Aircraft Analysis. *Mon. Wea. Rev.* **1995**, *123*, 944–969. [[CrossRef](#)]
31. Paegle, J.; Rasch, G.E. Three-Dimensional Characteristics of Diurnally Varying Boundary-Layer Flows. *Mon. Weather Rev.* **1973**, *101*, 746–756. [[CrossRef](#)]
32. Carrera, M.L.; Gyakum, J.R.; Lin, C.A. Observational Study of Wind Channeling within the St. Lawrence River Valley. *J. Appl. Meteorol. Clim.* **2009**, *48*, 2341–2361. [[CrossRef](#)]

Disclaimer/Publisher's Note: The statements, opinions and data contained in all publications are solely those of the individual author(s) and contributor(s) and not of MDPI and/or the editor(s). MDPI and/or the editor(s) disclaim responsibility for any injury to people or property resulting from any ideas, methods, instructions or products referred to in the content.